AIAA JOURNAL
Vol. 46, No. 8, August 2008

Nonlinear Frequency-Domain Analysis of Unsteady Flows in Turbomachinery with Multiple Excitation Frequencies

Kivanc Ekici* and Kenneth C. Hall†
Duke University, Durham, North Carolina 27708-0300

DOI: 10.2514/1.26006

A harmonic balance technique for the analysis of nonlinear unsteady flows in turbomachinery arising from several excitation sources, possibly with frequencies with irrational ratios, is presented in this paper. This method uses a mixed time-domain/frequency-domain approach that allows one to model the blade row on a computational grid spanning just a single blade passage, no matter the interblade phase angles of the original disturbances. Using this approach, we compute several solutions, each one corresponding to one of several times spanning one period for periodic flows or over a representative time interval for aperiodic flows. These time levels are coupled through a spectral time-derivative operator in the interior of the computational domain and through the far-field and periodic boundary conditions around the boundary of the domain. In this paper, we apply the method to the two-dimensional Euler equations (although the method can be applied to three-dimensional and viscous flows) and examine the nonlinear interaction of wake passing with blade vibration.

Nomenclature

$\boldsymbol{A}_k$, $\boldsymbol{B}_k$	=	kth temporal Fourier coefficients
$\boldsymbol{A}_{nm}$, $\boldsymbol{B}_{nm}$	=	nmth temporal Fourier coefficients
c	=	chord
$\mathbf{D}$	=	pseudospectral operator
E	=	total energy
$\mathbf{E}$, $\mathbf{E}^{-1}$	=	discrete inverse Fourier and Fourier transformation matrices
$\mathbf{E}^{+}$	=	pseudoinverse of $\mathbf{E}$ transformation matrix
$\boldsymbol{F}$, $\boldsymbol{G}$	=	flux vectors
f	=	velocity defect distribution
$\dot{f}$, $\dot{g}$	=	grid velocity due to unsteady blade motion
G	=	blade-to-blade gap
G_s	=	incoming wake gap
h_0	=	amplitude of plunging motion
h	=	enthalpy
N_k	=	nodal diameter for kth mode
p	=	pressure
q	=	total velocity
T	=	period of excitation
t	=	time
U	=	relative inflow velocity
$\boldsymbol{U}$	=	vector of conservation variables
$\boldsymbol{U}^*$	=	vector of conservation variables in all subtime levels
$\tilde{\boldsymbol{U}}$	=	vector of Fourier coefficients
u, v	=	Cartesian velocities
x, y	=	Cartesian coordinates
α	=	inlet wake angle
γ	=	specific heat ratio
ρ	=	density
σ	=	interblade phase angle
τ	=	pseudotime
Ω	=	excitation frequency
ω	=	excitation frequency

Presented as Paper 2995 at the 24th AIAA Applied Aerodynamics Conference, San Francisco, California, 5–8 June 2006; received 19 June 2006; revision received 29 January 2008; accepted for publication 18 April 2008.

*Research Associate, Department of Mechanical Engineering and Materials Science. Senior Member AIAA.

†Julian Francis Abele Professor, Department of Mechanical Engineering and Materials Science. Associate Fellow AIAA.

Introduction

HALL et al. [1,2] proposed the harmonic balance technique, a computationally efficient technique for computing complex time-periodic flows. Since then, a number of investigators have used the technique to model a number of interesting unsteady flows. Chen et al. [3] and Vilmin et al. [4] developed efficient nonlinear harmonic balance methods for predicting unsteady interaction of blade rows in turbomachinery. McMullen et al. [5,6] used the approach to investigate the flow around a cylinder and a pitching airfoil. Nadarajah et al. [7] applied the technique to an adjoint-based design code and found that the computational time was greatly reduced compared with their time-accurate code. Van der Weide et al. [8] used this technique in turbomachinery forced-response computations in which the rotor and stator rows had equal blade counts and showed that engineering accuracy can be obtained with as few as 11 subtime levels per blade passing. Gopinath and Jameson [9] used the harmonic balance technique and obtained efficient and accurate solutions for pitching airfoils and wings. Gopinath et al. [10] also used this technique to investigate the unsteady forced-response phenomenon in multistage turbomachinery. Thomas et al. [11,12] used a harmonic balance method to study the nonlinear aerodynamic effects on flutter and limit-cycle oscillations for airfoils and wings. Thomas et al. [13] also developed a discrete adjoint code for computing steady and unsteady aerodynamic design sensitivities for compressible viscous flows about airfoil configurations in which the nominal flow solver was based on a harmonic balance solution technique. Welch et al. [14] used the harmonic balance technique to accurately and efficiently solve the incompressible Navier–Stokes equations to model (pulsating) synthetic jets in quiescent crossflows and compared their results with hot-wire data. Breard [15] developed a similar frequency-domain model of the Euler equations for sound propagation and radiation of lined ducts that resulted in the less expensive approach to the calculations of noise propagation about a mean flow.

All of these previous methods have been limited to time-periodic flows. A number of interesting physical flows, however, are aperiodic. In turbomachinery, a blade row may be subjected to wake excitation at one frequency, whereas the airfoil vibrates at another. If the ratio of these excitation frequencies is irrational, then the flow will be aperiodic. Thus, the fundamental assumption of harmonic balance (i.e., that the flow is temporally periodic) fails. Recently

Ekici and Hall [16,17] have developed a variation of the harmonic balance technique that can model unsteady aperiodic flows.

In this paper, we use this technique to examine the nonlinear interaction of unsteady wakes with blade vibrations. We show that nonlinear effects play an important role in the migration of wakes through a row of turbine blades.

Unsteady Flow Modeling

Governing Equations

To motivate the present harmonic balance method, we apply the method to the two-dimensional Euler equations. However, in the computer code MUSTANG (Multistage Unsteady Analysis) developed at Duke University, the method is implemented for the three-dimensional Navier–Stokes equations.

The two-dimensional unsteady Euler equations can be written in conservation form as

$$\frac{\partial \boldsymbol{U}}{\partial t} + \frac{\partial \boldsymbol{F}}{\partial x} + \frac{\partial \boldsymbol{G}}{\partial y} = \boldsymbol{0} \tag{1}$$

where the vector of conservation variables $\boldsymbol{U}$ and the flux vectors $\boldsymbol{F}$ and $\boldsymbol{G}$ are given by

$$\boldsymbol{U} = \begin{bmatrix} \rho \\ \rho u \\ \rho v \\ \rho E \end{bmatrix}, \qquad \boldsymbol{F} = \begin{bmatrix} \rho u - \rho \dot{f} \\ \rho u^2 + p - \rho u \dot{f} \\ \rho uv - \rho v \dot{f} \\ \rho uh - \rho E \dot{f} \end{bmatrix}$$
$$\boldsymbol{G} = \begin{bmatrix} \rho v - \rho \dot{g} \\ \rho uv - \rho u \dot{g} \\ \rho v^2 + p - \rho v \dot{g} \\ \rho vh - \rho E \dot{g} \end{bmatrix} \tag{2}$$

In Eq. (2), $\dot{f}$ and $\dot{g}$ are, respectively, the x and y components of the velocity of the unsteady grid motion. In addition, the enthalpy is defined as

$$h = \frac{\rho E + p}{\rho} = \frac{\gamma}{\gamma - 1}\frac{p}{\rho} + \frac{1}{2}(u^2 + v^2)$$

Harmonic Balance Equations

Previously, Ekici and Hall [17] developed a harmonic balance method for computing unsteady aerodynamic flows in turbomachinery in which there exist two sources of excitation of different periods (e.g., wake passing and blade vibration). The salient features of that analysis are presented here for completeness.

Assume that there are two excitations in the flowfield with fundamental frequencies Ω_1 and Ω_2 and corresponding interblade phase angles σ_1 and σ_2, respectively. For each excitation, the periods can be written as $T_1 = 2\pi/\Omega_1$ and $T_2 = 2\pi/\Omega_2$. The ratio of the excitation frequencies in this analysis need not be rational. In other words, the combined unsteady excitation may be aperiodic in time. With this assumption, one can represent the unsteady flow quantities in the time domain with a real Fourier series given by

$$\boldsymbol{U}(t) = \sum_{n=0}^{\infty}\sum_{m=0}^{\infty} \boldsymbol{A}_{nm}\cos[(\Omega_1 n + \Omega_2 m)t] + \boldsymbol{B}_{nm}\sin[(\Omega_1 n + \Omega_2 m)t] \tag{3}$$

where $\boldsymbol{A}_{nm}$ and $\boldsymbol{B}_{nm}$ are the Fourier coefficients of the conservation variables.

Theoretically, n and m can take on an infinite number of integer values. In practice, only a handful of the many possible Fourier modes contribute significantly to the nonlinear solution of the flowfield, and thus the series in Eq. (3) can be truncated. Thus, one must decide which (n, m) combinations to keep in the harmonic balance analysis. The selection of the Fourier modes is more art than science. However, there are some rules we follow. First, one must always include the mode $n = m = 0$, because it represents the mean flow. Second, one must retain the fundamental mode (blade vibration for flutter and wake passing for forced response) and its higher harmonics for each individual excitation. Finally, one must include the cross terms, especially those with low frequencies and low interblade phase angles, which make the interaction between different excitations possible. Having selected the modes, the original Fourier series [Eq. (3)] can be approximated by

$$\boldsymbol{U}(t) \approx \boldsymbol{A}_0 + \sum_{k=1}^{N} \boldsymbol{A}_k \cos(\omega_k t) + \boldsymbol{B}_k \sin(\omega_k t) \tag{4}$$

where N is the number of modes in the model; ω_k is the frequency of the kth mode; and $\boldsymbol{A}_0$, $\boldsymbol{A}_k$, and $\boldsymbol{B}_k$ are the Fourier coefficients of the kth mode. As an example, Table 1 shows typical harmonics kept for a two-excitation-frequency case.

In the present computational method, we store the conservation variables in each blade row at a number of subtime levels. Assembled together into one vector, these solutions are denoted by the vector $\boldsymbol{U}^*$; in addition, we denote the vector of Fourier coefficients by $\tilde{\boldsymbol{U}}$: that is,

$$\boldsymbol{U}^* = \begin{Bmatrix} \boldsymbol{U}_1 \\ \boldsymbol{U}_2 \\ \boldsymbol{U}_3 \\ \boldsymbol{U}_4 \\ \vdots \end{Bmatrix}, \qquad \tilde{\boldsymbol{U}} = \begin{Bmatrix} \boldsymbol{A}_0 \\ \boldsymbol{A}_1 \\ \boldsymbol{A}_2 \\ \vdots \\ \boldsymbol{B}_1 \\ \boldsymbol{B}_2 \\ \vdots \end{Bmatrix} \tag{5}$$

For temporally periodic flows, the Fourier coefficients can be determined from the subtime level solutions by a discrete Fourier transform. Conversely, the conservation variables at the subtime level can be determined from the Fourier coefficients by the inverse discrete Fourier transform. These relations can be written as

$$\tilde{\boldsymbol{U}} = \mathbf{E}^{-1}\boldsymbol{U}^* \tag{6}$$

$$\boldsymbol{U}^* = \mathbf{E}\tilde{\boldsymbol{U}} \tag{7}$$

where $\mathbf{E}$ is the inverse discrete Fourier transform operator written in matrix form. Note that $\mathbf{E}$ is a square matrix because the number of time sublevels is equal to the number of Fourier coefficients.

For aperiodic flows, the situation is slightly more complicated. The flow is no longer periodic. Nevertheless, one can still determine the Fourier coefficients from information at time sublevels. However, some care must be taken to ensure that the aperiodic equivalents of Eqs. (6) and (7) are well-conditioned. First, the period spanned by the time sublevels and their spacing must be such that the Fourier coefficients are observable. We typically use about 50% more time levels than the number of Fourier coefficients for aperiodic flows. Equation (7) is essentially unchanged, except that $\mathbf{E}$ is no longer square: it now has more rows than columns. Second, Eq. (6) is replaced by

$$\tilde{\boldsymbol{U}} = \mathbf{E}^{+}\boldsymbol{U}^* \tag{8}$$

Table 1 Typical harmonics kept for a two-excitation-frequency case

k	(n, m)	ω_k	$\bar{\sigma}_k$
1	(1, 0)	Ω_1	σ_1
2	(2, 0)	$2\Omega_1$	$2\sigma_1$
3	(0, 1)	Ω_2	σ_2
4	(0, 2)	$2\Omega_2$	$2\sigma_2$
5	(1, 2)	$\Omega_1 + 2\Omega_2$	$\sigma_1 + 2\sigma_2$
6	(1, 1)	$\Omega_1 + \Omega_2$	$\sigma_1 + \sigma_2$

where $\mathbf{E}^+$ denotes the pseudoinverse of $\mathbf{E}$. Using the example in Table 1 with $3N + 1$ time levels, Eq. (4) can be written in matrix-vector form as

$$\begin{Bmatrix} \boldsymbol{U}_1 \\ \boldsymbol{U}_2 \\ \boldsymbol{U}_3 \\ \vdots \\ \boldsymbol{U}_{19} \end{Bmatrix} = \underbrace{\begin{bmatrix} 1 & \cos\omega_1 t_1 & \cdots & \cos\omega_6 t_1 & \sin\omega_1 t_1 & \cdots & \sin\omega_6 t_1 \\ 1 & \cos\omega_1 t_2 & \cdots & \cos\omega_6 t_2 & \sin\omega_1 t_2 & \cdots & \sin\omega_6 t_2 \\ 1 & \cos\omega_1 t_3 & \cdots & \cos\omega_6 t_3 & \sin\omega_1 t_3 & \cdots & \sin\omega_6 t_3 \\ \vdots & & & & & & \\ 1 & \cos\omega_1 t_{19} & \cdots & \cos\omega_6 t_{19} & \sin\omega_1 t_{19} & \cdots & \sin\omega_6 t_{19} \end{bmatrix}}_{\mathbf{E}} \times \begin{Bmatrix} \boldsymbol{A}_0 \\ \boldsymbol{A}_1 \\ \vdots \\ \boldsymbol{A}_6 \\ \boldsymbol{B}_1 \\ \vdots \\ \boldsymbol{B}_6 \end{Bmatrix} \tag{9}$$

Having described the kinematics of the flow, we now turn our attention to the development of the harmonic balance equations. In conservation form, the Euler equations are given by Eq. (1). Note that Eq. (1) contains four equations: one conservation-of-mass equation, two conservation-of-momentum equations, and one conservation-of-energy equation. Next, we write these equations at all subtime levels simultaneously, so that

$$\frac{\partial \boldsymbol{U}^*}{\partial t} + \frac{\partial \boldsymbol{F}^*}{\partial x} + \frac{\partial \boldsymbol{G}^*}{\partial y} = \mathbf{0} \tag{10}$$

where, for example, $\boldsymbol{F}^*$ is the vector of x fluxes evaluated at $\boldsymbol{U}^*$. Hence, Eq. (10) has $4 \times M$ equations, where M is the number of subtime levels.

Note that the M sets of conservation equations in Eq. (10) are coupled only through the time-derivative term, which is approximated by the pseudospectral operator $\mathbf{D}$. To motivate the development of $\mathbf{D}$, we note that

$$\frac{\partial}{\partial t}\boldsymbol{U}^* = \sum_{k=1}^{N} [-\omega_k \cdot \boldsymbol{A}_k \sin(\omega_k t) + \omega_k \cdot \boldsymbol{B}_k \cos(\omega_k t)] \tag{11}$$

or, in matrix form,

$$\frac{\partial \boldsymbol{U}^*}{\partial t} = \frac{\partial \mathbf{E}}{\partial t}\tilde{\boldsymbol{U}} \tag{12}$$

Making use of Eq. (8) gives the desired pseudospectral operator:

$$\frac{\partial \boldsymbol{U}^*}{\partial t} = \frac{\partial \mathbf{E}}{\partial t}\mathbf{E}^+\boldsymbol{U}^* = \mathbf{D}\boldsymbol{U}^* \tag{13}$$

Finally, substitution of Eq. (13) into Eq. (10) gives the desired harmonic balance equations: that is,

$$\mathbf{D}\,\boldsymbol{U}^* + \frac{\partial \boldsymbol{F}^*}{\partial x} + \frac{\partial \boldsymbol{G}^*}{\partial y} = \mathbf{0} \tag{14}$$

Numerical Integration

Having selected the time levels, we next solve Eq. (14). Note that Eq. (14) is mathematically a steady equation: that is, time does not appear explicitly. To solve the equations using conventional time-marching techniques, we introduce a pseudotime term [18], so that

$$\frac{\partial \boldsymbol{U}^*}{\partial \tau} + \mathbf{D}\boldsymbol{U}^* + \frac{\partial \boldsymbol{F}^*}{\partial x} + \frac{\partial \boldsymbol{G}^*}{\partial y} = \mathbf{0} \tag{15}$$

Equation (15) is then marched in pseudotime until convergence. When converged, the added pseudotime term goes to zero, and the harmonic balance equation [Eq. (14)] is recovered. Because only the steady-state solution of Eq. (15) is desired, acceleration techniques such as multiple-grid acceleration can be used to speed convergence.

The current approach is somewhat similar to the dual-time-step approach [19,20], except that in the harmonic balance method, several time levels are stored. In the dual-time-step approach, one marches the solution from one physical time level to the next. Within each of these time steps, a number of pseudotime steps are taken to improve the accuracy of the physical time-stepping solution. In the harmonic balance technique, on the other hand, all physical time levels are computed simultaneously, with pseudotime marching used to drive the solution to convergence. The various physical time levels are only coupled through the complex blade-to-blade boundary conditions and through a pseudospectral operator that approximates the time derivatives in the Euler or Navier–Stokes equations. The main advantage of this modified harmonic balance approach is that the computational cost scales (nearly) linearly with the number of time levels retained in the model. In addition, the complex blade-to-blade boundary conditions allow one to model the aperiodic unsteady flow on a grid spanning a single blade passage. On the other hand, in dual-time-step approach, one needs to model the aperiodic flow for the entire wheel and to run many small time steps for a number of revolutions, which dramatically increases the required computational time. Furthermore, use of the pseudospectral time-derivative operator allows one to use a small number of time levels (or equivalently harmonics) to obtain quite accurate solutions.

As mentioned previously, Eq. (15) is discretized on a computational grid spanning a single blade passage in each blade row. A typical (two-dimensional) grid is shown in Fig. 1. We use Ni's [21] Lax–Wendroff scheme to discretize the harmonic balance equations, with multiple-grid acceleration to speed convergence.

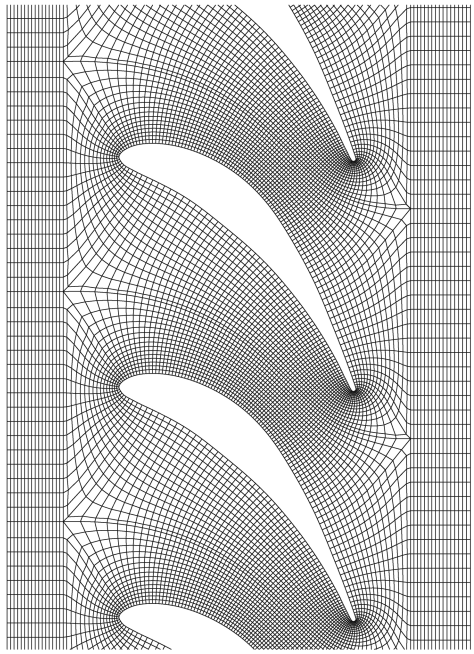

Fig. 1 Computational grid for Cambridge turbine number 2 geometry [24,26]. Computations are performed in a single blade passage. Multiple passages are shown for clarity.

Note that the solution of the harmonic balance equations is similar to the solution of the steady Euler equations. The vector of conservation variables and the flux vectors are somewhat larger, but the flux vectors are computed in the usual way at each time level. The equations at each time level are coupled by the pseudospectral time-derivative term, which appears as an additional source term.

Periodic Boundary Condition

The computational domain can be reduced to a single blade passage within each blade row by making use of complex periodicity conditions along the periodic boundaries. To apply these conditions, the solution $\boldsymbol{U}^*$ is transformed along the periodic boundaries using Eq. (6) to find the vector of Fourier coefficients $\tilde{\boldsymbol{U}}$ (which contains the cosine and sine coefficients $\boldsymbol{A}_k$ and $\boldsymbol{B}_k$). Inspection of Eqs. (3) and (4) reveals that the appropriate boundary conditions are given by

$$\boldsymbol{A}_k(x, y+G) = \boldsymbol{A}_k(x, y) \cdot \cos(N_k G) - \boldsymbol{B}_k(x, y) \cdot \sin(N_k G) \quad (16)$$

$$\boldsymbol{B}_k(x, y+G) = \boldsymbol{A}_k(x, y) \cdot \sin(N_k G) + \boldsymbol{B}_k(x, y) \cdot \cos(N_k G) \quad (17)$$

These boundary conditions, similar to those developed by He and Denton [22] and He [23] for time-accurate time-marching flow solvers, are applied at every iteration of the Lax–Wendroff solver.

Results

In this paper, we consider the response of a turbine blade row subjected to wake/rotor interaction and blade vibration, both individually and in combination. We consider the turbine studied by Hodson [24,25] both computationally and experimentally. The computational grid used in this study, shown in Fig. 1, is a block-structured grid containing 3584 computational cells. For the cases considered in this paper, the (nondimensional) steady inlet total pressure and the steady inlet total density are 1.0. The blade-to-blade inlet flow angle is 2 deg, and the exit pressure is 0.896. These conditions correspond to inlet and exit Mach numbers of 0.146 and 0.400 [26], respectively.

First, we computed the steady flow through the turbine without any unsteady excitation (blade vibration or incident wakes). Shown in Fig. 2 is the computed velocity on the surface of the airfoil. Also shown for comparison is the measured surface velocity, as reported by Hodson [24,25]. The results of the present analysis are seen to be in excellent agreement with the experimental data.

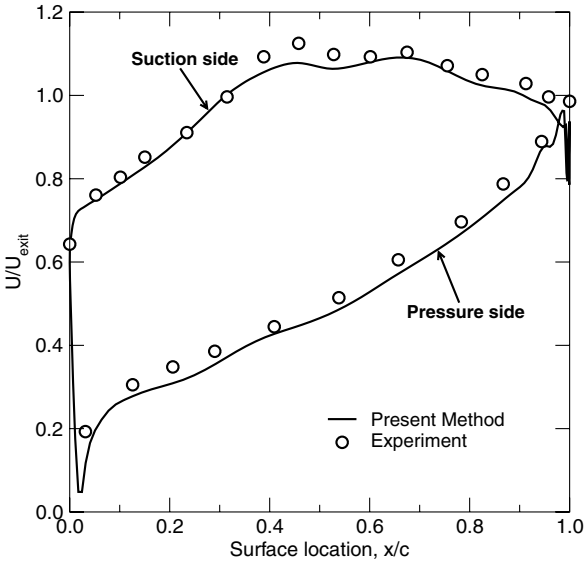

Fig. 2 Velocity distribution of the surface of Cambridge turbine number 2. Shown is the experimental data due to Hodson [25], and the computed results using the present method.

Next, we used the present harmonic balance method to compute the unsteady flow through the turbine due to a wake from an upstream blade row. Here, we use a definition of the wake similar to that used in Giles's [26] calculations, except that we prescribe a higher temperature wake. In this model, the static pressure is uniform, the periodic velocity defect is prescribed, and the wake flow is parallel in the stator frame of reference. Here, the wake is defined by

$$\begin{aligned} p_w &= p_s \qquad u_w = q_s[1 - f(\eta)]\cos(\alpha_s) \\ v_w &= q_s[1 - f(\eta)]\sin(\alpha_s) \qquad \rho_w = \rho_s[1 - f(\eta)] \end{aligned} \quad (18)$$

where the subscript w denotes the wake values at the inlet, s denotes the inlet steady values, q_s is the total steady velocity, α_s is the inlet wake angle, and $f(\eta)$ is a periodic function that defines the velocity defect distribution, where η is defined as

$$\eta = \frac{y - \tan(\alpha_s)x}{G_s} \quad (19)$$

In this paper, we use a wake velocity defect of 20%, a wake width of 0.15, and a wake angle of 64 deg. Further details about the wake model can be found in [26]. Note that although there is probably more interest in a turbine with a cooled upstream wake, we chose a hot wake because previous numerical analyses [24,26] for this geometry were performed for a hot incoming wake.

For this series of computations, we computed the flow in a single blade passage using 11 time levels or, equivalently, five harmonics of the wake passing frequency. Figure 3 shows the computed results. Shown are the unsteady velocity vectors and contours of entropy within the blade row. Note that for the contour plots presented in this paper, a darker contour level corresponds to a higher value of the flow quantity. The velocity vectors are plotted with the mean velocity component subtracted to better visualize the unsteady component of the velocity field. Recall that the solution is computed in a single blade passage. For clarity in plotting, the solution is reconstituted and plotted in several blade passages at a single instant in time. Plotted in this way, the wake is clearly seen, including the so-called negative jet in the wake arising from the velocity defect in the wake. As pointed out by Kerrebrock and Mikolajczak [27], this negative jet convects the high-entropy wake toward the suction surface of the turbine blades, as can be clearly seen in the entropy contours. Fluid in the wake is self-convected toward, and accumulates on, the suction surface. Conversely, the low-entropy fluid outside the wake accumulates on the pressure surface of the airfoil. Note that qualitatively, these results are in good agreement with the analyses of Hodson [24] and Giles [26].

The fact that fluid from the wake is convected toward the suction surface of the airfoils can also be seen in Fig. 4. Shown are contours of the mean (time-averaged) pressure and entropy. The mean pressure in this example is very nearly indistinguishable from the pressure calculated with no wake at all. However, the mean migration of the high-entropy (hot) fluid in the wake depends fundamentally on the unsteady flowfield. We see in Fig. 4 that the effect of the unsteadiness in the flow is to migrate the hot fluid toward the suction side of the airfoil and the cooler fluid outside of the wake toward the pressure side. Thus, for the purposes of computing the mean pressure loads, one can (in this case) ignore unsteady effects. However, the mean value of the flow quantities that are convected, such as entropy and vorticity, depend fundamentally on unsteady flow processes.

Next, we consider the effect of two sources of unsteadiness and their potential nonlinear interactions. In time-linearized theories, the sources of unsteadiness would be considered small and superposable and thus would not interact. In the present nonlinear harmonic balance analysis, however, we can easily study nonlinear interactions, even those that occur at nonintegral frequencies or at different interblade phase angles. Here, we consider the case of the prescribed wake as before, but now include a vibratory motion of the turbine blades. For the case considered here, we assume a plunging motion of the airfoil normal to the chord of the airfoil with an amplitude h_0 equal to 0.0, 2.0, or 10.0% of the chord, with a reduced

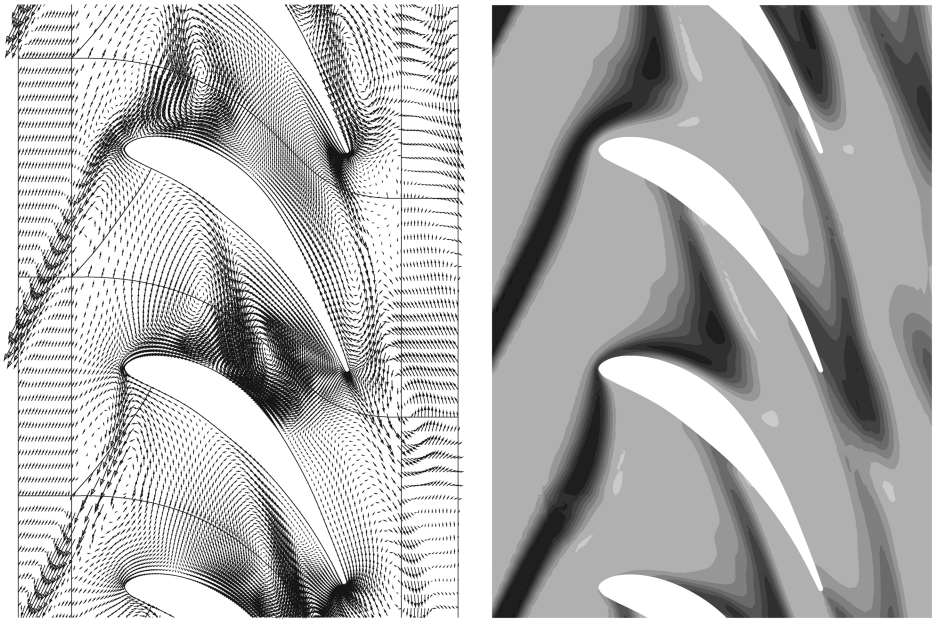

Fig. 3 Computed unsteady velocity vectors (left) and entropy contours (right) in Cambridge turbine number 2 for the case of a prescribed incoming wake.

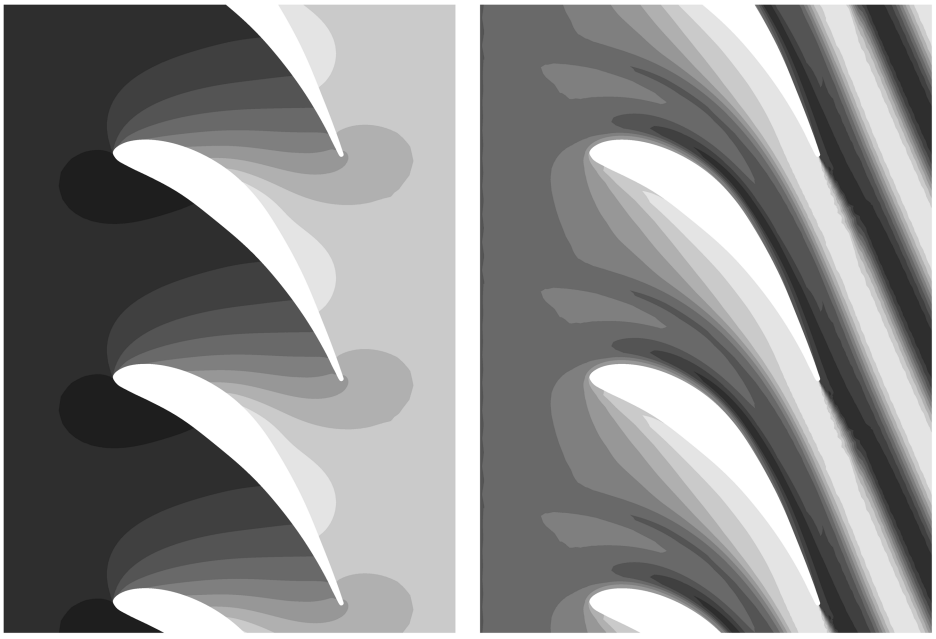

Fig. 4 Computed mean pressure (left) and mean entropy (right) contours in Cambridge turbine number 2 for the case of a prescribed incoming wake.

frequency $\bar{\omega} = \omega c/(2U_{\text{axial}})$ of 0.5 and an interblade phase angle σ of 90 deg. By way of comparison, the reduced frequency and interblade phase angle of the wake is $\bar{\omega} = 4.5$ and $\sigma = 254$ deg, respectively. Here, we used 31 subtime levels with 10 discrete frequencies.

Shown in Fig. 5 is the computed mean (time-averaged) pressure distribution on the surface of the turbine blade with various combinations of wake excitation and blade vibration. We see that the time-averaged pressure distribution in all cases is very nearly equal to the steady pressure distribution computed with no sources of unsteadiness. Some very small differences between the mean flow and steady flow near the leading edge are seen only for the largest levels of blade vibration.

Similarly, Fig. 6 shows the computed mean flow entropy on the surface of the airfoil. (Admittedly, such calculations should be computed using a Navier–Stokes model, because an inviscid adiabatic model should predict infinitely thin layers of high and low entropy near the surface of the airfoil [28,29]. However, small amounts of artificial viscosity in the flow solver mimic the effect of actual viscosity and effectively eliminate this spurious layering effect. The entropy shown in Fig. 6 should be regarded as the entropy at the edge of the boundary layer.) Now note the importance of unsteady effects on the time-averaged flow quantities. First consider the effect of the wake alone. One sees that because of the negative jet velocities in the wake, high-entropy (hot) fluid piles up on the aft portion of the suction surface of the airfoil. Conversely, low-entropy (cool) fluid is convected onto the pressure surface. If one now introduces a small amount of blade vibration ($h/c = 0.02$), the results are essentially unchanged. In other words, small amounts of blade vibration do not interact nonlinearly with the wake excitation. On the other hand, one sees that large-amplitude blade motions ($h_0/c = 0.10$) do, in fact, change the mean distribution of the entropy on the airfoil surface quite significantly. In other words, for the purpose of computing mean flow quantities, nonlinear interactions of unsteadiness in the flow may be important.

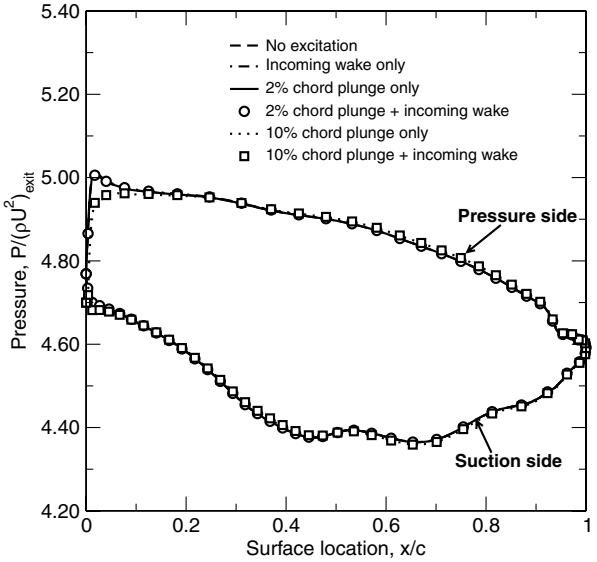

Fig. 5 Computed mean pressure distribution on the surface of the Cambridge turbine number 2 blade surface for various combinations of wake excitations and blade vibrations.

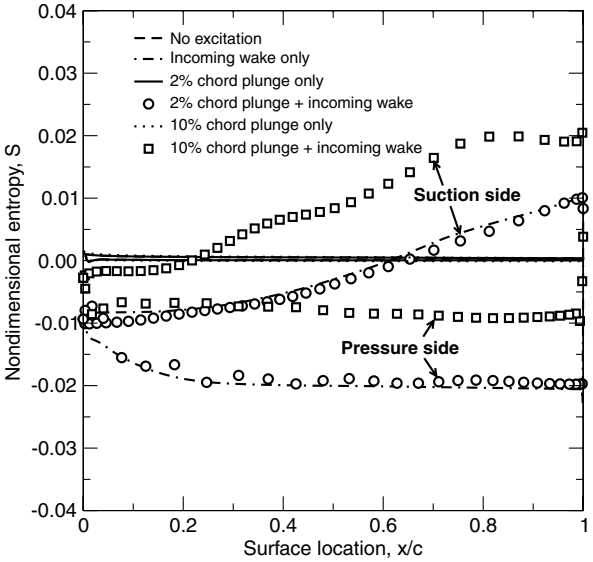

Fig. 6 Computed mean entropy distribution on the surface of the Cambridge turbine number 2 blade surface for various combinations of wake excitations and blade vibrations.

For aeromechanic applications, it is the unsteady pressure acting on the airfoil surface at the frequency of airfoil vibration that is important, because only those forces that are integer multiples (true harmonics) of the vibratory frequency of the airfoil do aeromechanical work. Forces that are noninteger multiples of the fundamental vibration frequency may do work over a single cycle. However, over many cycles, they do no average work. Figure 7 shows the Fourier component of the computed unsteady pressures on the surface of the airfoil at the frequency of the blade vibration. Shown are the real and imaginary parts of the pressure normalized by the amplitude of the blade vibration, computed for several combinations of wake excitation and blade vibration. Note in all cases that the pressure distributions are very nearly linear (that is, the unsteady pressures scale with the vibratory amplitude) and there is a noticeable but weak influence of the wake. In other words, for aeromechanical applications (at least for the case considered here), nonlinear effects play only a minor role.

Next, we consider the unsteady entropy on the surface of the airfoil. Figure 8 shows the component of unsteady surface entropy *at the wake passing frequency*. Note that for small-amplitude blade vibrations ($h_0/c = 0.02$), the first harmonic of the unsteady entropy is the same as with no blade motion. However, for larger-amplitude blade vibrations ($h_0/c = 0.10$), the first harmonic is significantly modified.

Similarly, shown in Fig. 9 is the Fourier component of the entropy *at the vibratory frequency of the blades*. For both the small- and large-amplitude blade vibrations, we see significant levels of unsteady entropy. In other words, there is *crosstalk* between the wake passing and blade vibration frequencies; unsteady entropy perturbations are seen at frequencies that are not multiples of the wake passing frequency.

Having computed the unsteady flow for several model problems, we return to the issue of accuracy and mode convergence. In the preceding calculations, we used 11 time levels per period for the wake only calculations and 31 time levels for the wake/blade-motion computations. Shown in Fig. 10 is the computed surface entropy for the wake-alone case computed using 3, 5, 7, 9, and 11 time levels (1, 2, 3, 4, and 5 harmonics). Solutions for 2, 3, 4 and 5 harmonics are in good agreement, with only very minor differences. As one can see, retaining only one harmonic is not adequate. Thus, to accurately

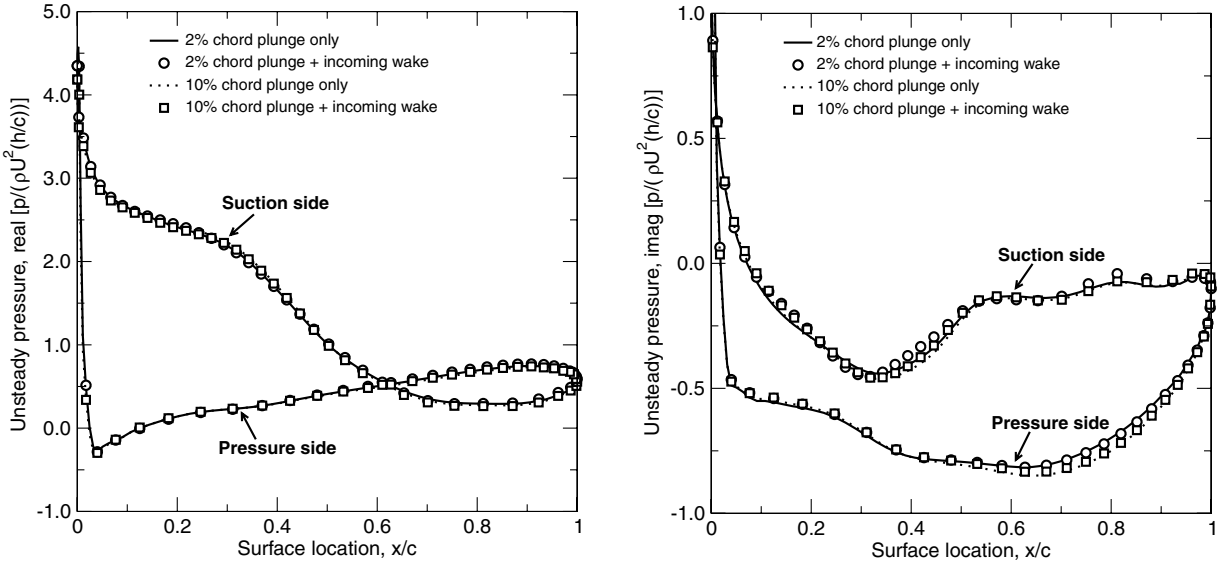

Fig. 7 Computed unsteady pressure distribution on the surface of the Cambridge turbine number 2 blade surface for various combinations of wake excitations and blade vibrations. Plotted is the Fourier component of the unsteady pressure at the blade vibration frequency.

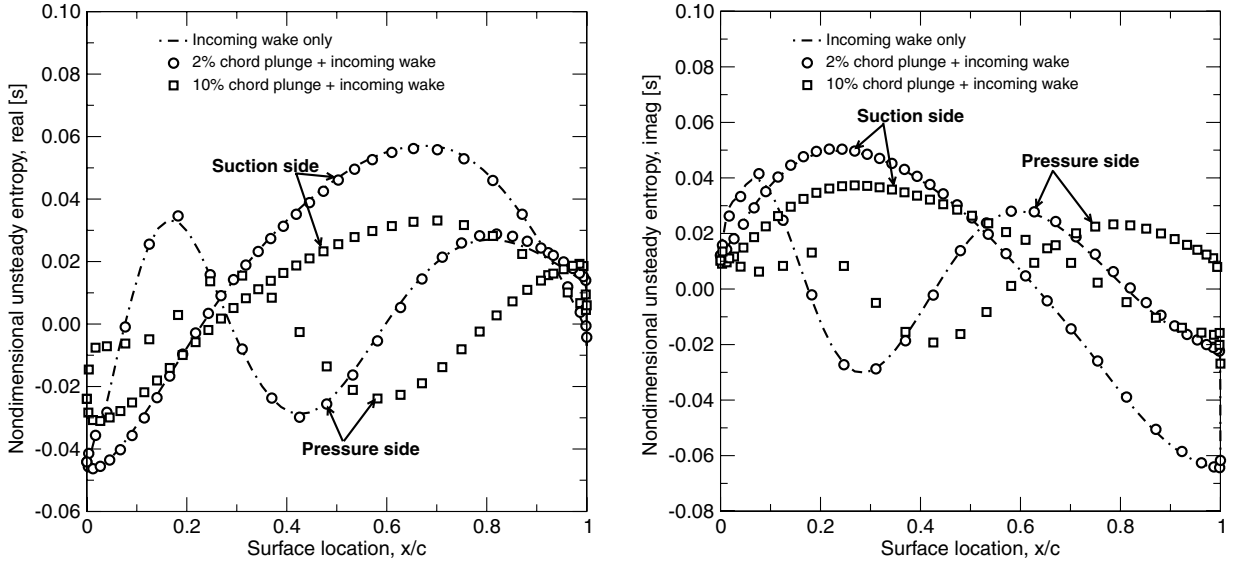

Fig. 8 Computed unsteady entropy distribution on the surface of the Cambridge turbine number 2 blade surface for various combinations of wake excitations and blade vibrations. Plotted is the Fourier component of the unsteady entropy at the wake passing frequency.

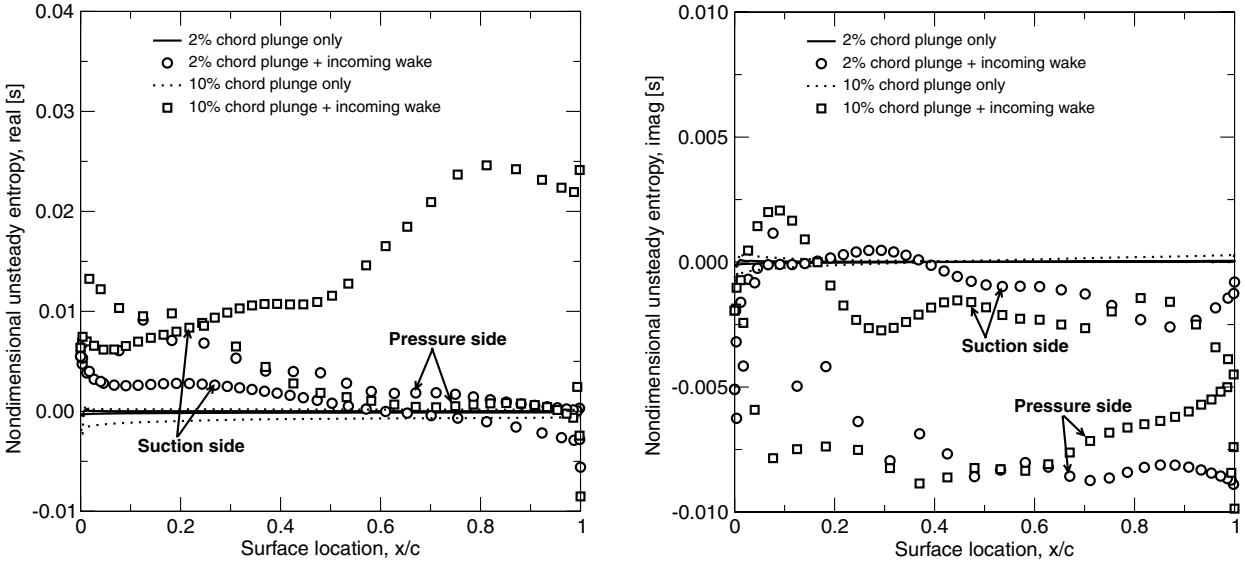

Fig. 9 Computed unsteady entropy distribution on the surface of the Cambridge turbine number 2 blade surface for various combinations of wake excitations and blade vibrations. Plotted is the Fourier component of the unsteady entropy at the blade vibratory frequency.

compute the effect of unsteadiness on the mean flow and the first harmonic of the unsteady flow, one only needs as few as two harmonics (five time levels).

Finally, we consider the computational efficiency of the present method. Figure 11 shows the convergence histories for the present harmonic balance method for the wake-interaction-only and blade-vibration-only problems with 11 subtime levels (five modes), the blade-vibration/wake-interaction problem with 25 subtime levels (eight modes), and the steady flow solver. Note that in all cases (periodic and aperiodic), around 12,000 iterations are required to achieve a converged solution and the solutions converge at about the same rate. Thus, the computational time required is approximately equal to the number of time levels in the model times the computational time required for a single steady flow calculation. Note, in particular, that the method benefits greatly from the fact that only a single blade passage is required, regardless of the combination of frequencies and interblade phase angles of the original disturbances, and from the fact that only a small number of subtime levels are needed to obtain accurate solutions. On the other hand, with a traditional time-accurate approach, one needs to model the aperiodic flow for the entire wheel and run many small time steps over a large number of revolutions, which dramatically increases the required computational time.

Conclusions

In this paper, we have presented a harmonic balance technique for computing unsteady flows in multistage turbomachinery. The method can efficiently model both *periodic* and *aperiodic* flows arising from different sources of unsteadiness. (The flow will be aperiodic if multiple sources of excitation are present with irrational frequency ratios.) The model is computationally efficient for several reasons. First, the computational domain can be reduced to a single blade passage regardless of the combination of frequencies and interblade phase angles of the original disturbances. Second, time derivatives are computed using a very accurate spectral operator, reducing the number of time levels that must be retained in the model. Third, we are often concerned with either mean flow (as opposed to steady flow) quantities or Fourier components of flow quantities acting at a single frequency. In these cases, only enough time levels

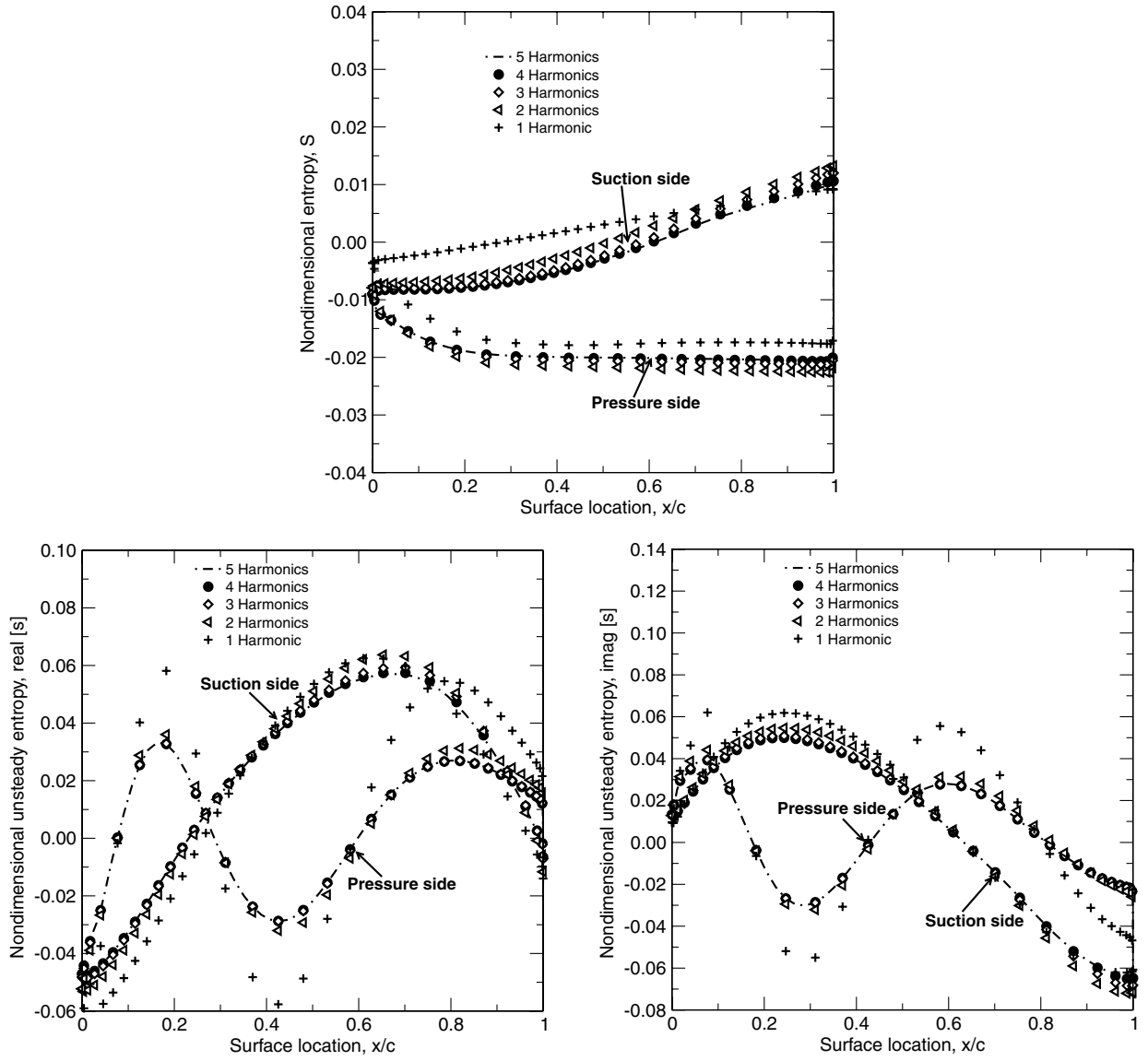

Fig. 10 Computed unsteady entropy distribution on the surface of the Cambridge turbine number 2 blade surface for wake excitation. Plotted is the Fourier component of the unsteady entropy at the wake passing frequency. Shown are solutions computed using different number of harmonics.

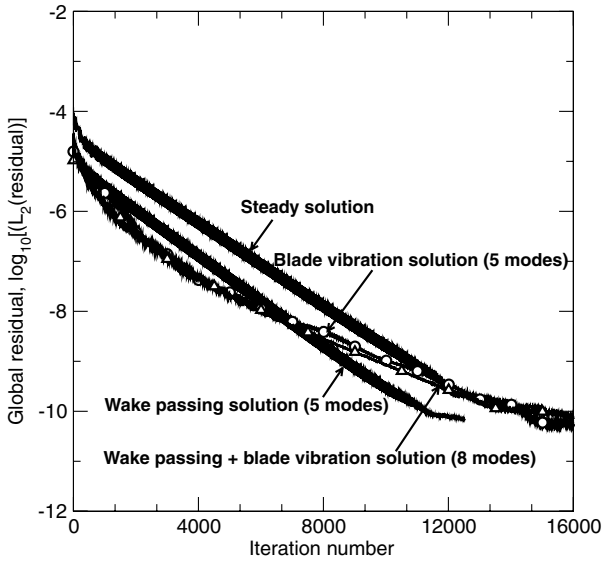

Fig. 11 Convergence histories for steady and unsteady flow calculations.

need to be retained to accurately model these flow components, again reducing the number of harmonics (and, equivalently, time levels) in the model.

The method is ideally suited for the computation of the aerodynamic forces that produce flutter and forced response in turbomachinery. Furthermore, the method can also be used effectively to model mean flow performance: for example, the effect of unsteadiness on mean heat transfer. We have shown that to accurately compute the effects of unsteadiness on the mean flow thermodynamic properties requires as few as two harmonics.

For the examples presented in this paper, nonlinear effects were relatively unimportant in the computation of steady and unsteady pressure loads, but important for the computation of wake migration in the turbine passage. We note that the use of the Euler equations to model wake migration does not account for the diffusion of the wake through viscous effects. However, the present method can be readily applied to the Navier–Stokes equations.

Acknowledgments

This work was sponsored by a grant from the NASA John H. Glenn Research Center at Lewis Field (NASA grant NAG3-2627) with technical oversight provided by Anatole Kurkov. Additional

support was provided by the Guide Consortium, with technical oversight provided by Jerry Griffin of Carnegie Mellon University.

References

[1] Hall, K. C., Thomas, J. P., and Clark, W. S., "Computation of Unsteady Nonlinear Flows in Cascades Using a Harmonic Balance Technique," *Proceedings of the 9th International Symposium on Unsteady Aerodynamics, Aeroacoustics and Aeroelasticity of Turbomachines*, edited by P. Ferrand and S. Aubert, Presses Univ. de Grenoble, Lyon, France, 2000, pp. 409–426.

[2] Hall, K. C., Thomas, J. P., and Clark, W. S., "Computation of Unsteady Nonlinear Flows in Cascades Using a Harmonic Balance Technique," *AIAA Journal*, Vol. 40, No. 5, May 2002, pp. 879–886.

[3] Chen, T., Vasanthakumar, P., and He, L., "Analysis of Unsteady Blade Row Interaction Using Nonlinear Harmonic Approach," *Journal of Propulsion and Power*, Vol. 17, No. 3, May–June 2001, pp. 651–658.

[4] Vilmin, S., Lorrain, E., Hirsch, C., and Swoboda, M., "Unsteady Flow Modeling Across the Rotor/Stator Interface Using the Nonlinear Harmonic Method," American Society of Mechanical Engineers Paper GT2006-90210, 2006.

[5] McMullen, M., Jameson, A., and Alonso, J. J., "Acceleration of Convergence to a Periodic Steady State in Turbomachinery Flows," AIAA Paper 2001-152, 2001.

[6] McMullen, M., Jameson, A., and Alonso, J. J., "Application of a Nonlinear Frequency Domain Solver to the Euler and Navier-Stokes Equations," AIAA Paper 2002-120, 2002.

[7] Nadarajah, S., McMullen, M., and Jameson, A., "Optimal Control of Unsteady Flows Using Time-Accurate and Non-Linear Frequency Domain Methods," AIAA Paper 2003-3875, 2003.

[8] Van der Weide, E., Gopinath, A., and Jameson, A., "Turbomachinery Applications with the Time Spectral Method," AIAA Paper 2005-4905, 2005.

[9] Gopinath, A., and Jameson, A., "Time Spectral Method for Periodic Unsteady Computations over Two- and Three-Dimensional Bodies," AIAA Paper 2005-1220, 2005.

[10] Gopinath, A., van der Weide, E., Alonso, J. J., Jameson, A., Ekici, K., and Hall, K. C., "Three-Dimensional Unsteady Multi-Stage Turbomachinery Simulations Using the Harmonic Balance Technique," AIAA Paper 2007-0892, 2007.

[11] Thomas, J. P., Dowell, E. H., and Hall, K. C., "Nonlinear Inviscid Aerodynamic Effects on Transonic Divergence, Flutter, and Limit-Cycle Oscillations," *AIAA Journal*, Vol. 40, No. 4, Apr. 2002, pp. 638–646.

[12] Thomas, J. P., Hall, K. C., and Dowell, E. H., "A Harmonic Balance Approach for Modeling Nonlinear Aeroelastic Behavior of Wings in Transonic Viscous Flow," AIAA Paper 2003-1924, 2003.

[13] Thomas, J. P., Hall, K. C., and Dowell, E. H., "Discrete Adjoint Approach for Modeling Unsteady Aerodynamic Design Sensitivities," *AIAA Journal*, Vol. 43, No. 9, Sept. 2005, pp. 1931–1936. doi:10.2514/1.731

[14] Welch, G., Milanovic, I., and Zaman, K., "Application of Harmonic Balance Technique to Synthetic Jets in Crossflow," AIAA Paper 2005-1111, 2005.

[15] Breard, C., "Acoustic Propagation and Radiation Modeling of Lined Duct with Linear and Non-Linear Frequency-Domain Solver," AIAA Paper 2003-3265, 2003.

[16] Ekici, K., and Hall, K. C., "Nonlinear Analysis of Unsteady Flows in Multistage Turbomachines Using the Harmonic Balance Technique," AIAA Paper 2006-422, 2006.

[17] Ekici, K., and Hall, K. C., "Nonlinear Analysis of Unsteady Flows in Multistage Turbomachines Using Harmonic Balance," *AIAA Journal*, Vol. 45, No. 5, May 2007, pp. 1047–1057. doi:10.2514/1.22888

[18] Ni, R. H., and Sisto, F., "Numerical Computation of Nonstationary Aerodynamics of Flat Plate Cascades in Compressible Flow," *Journal of Engineering for Power*, Vol. 98, No. 2, Apr. 1976, pp. 165–170.

[19] Jameson, A., "Time-Dependent Calculations Using Multigrid with Application to Unsteady Flows Past Airfoils and Wings," AIAA Paper 91-1596, 1991.

[20] Davis, R. L., Shang, T., Buteau, J., and Ni, R. H., "Prediction of 3-D Unsteady Flow in Multi-Stage Turbomachinery Using an Implicit Dual Time-Step Approach," AIAA Paper 96-2565, 1996.

[21] Ni, R. H., "A Multiple-Grid Scheme for Solving the Euler Equations," *AIAA Journal*, Vol. 20, No. 11, Nov. 1982, pp. 1565–1571.

[22] He, L., and Denton, J. D., "Three-Dimensional Time-Marching Inviscid and Viscous Solutions for Unsteady Flows Around Vibrating Blades," *Journal of Turbomachinery*, Vol. 116, No. 3, July 1994, pp. 469–476.

[23] He, L., "Method of Simulating Unsteady Turbomachinry Flows with Multiple Perturbations," *AIAA Journal*, Vol. 30, No. 11, Nov. 1992, pp. 2730–2735.

[24] Hodson, H., "An Inviscid Blade-to-Blade Prediction of a Wake-Generated Unsteady Flow," *Journal of Engineering for Gas Turbines and Power*, Vol. 107, Apr. 1985, pp. 337–343.

[25] Hodson, H., "Measurements of Wake-Generated Unsteadiness in the Rotor Passages of Axial Turbines," *Journal of Engineering for Gas Turbines and Power*, Vol. 107, Apr. 1985, pp. 467–476.

[26] Giles, M. B., "Calculation of Unsteady Wake/Rotor Interaction," *Journal of Propulsion and Power*, Vol. 4, No. 4, July–Aug. 1988, pp. 356–362.

[27] Kerrebrock, J. L., and Mikolajczak, A. A., "Intra-Stator Transport of Rotor Wakes and Its Effect on Compressor Performance," *Journal of Engineering for Power*, Vol. 92, No. 4, 1970, pp. 359–368.

[28] Hall, K. C., and Verdon, J. M., "Gust Response Analysis for Cascades Operating in Nonuniform Mean Flows," *AIAA Journal*, Vol. 29, No. 9, 1991, pp. 1463–1471.

[29] Atassi, H. M., and Grzedzinski, J., "Unsteady Disturbances of Streaming Motions Around Bodies," *Journal of Fluid Mechanics*, Vol. 209, Dec. 1989, pp. 385–403. doi:10.1017/S0022112089003150

K. Ghia
Associate Editor